Orbital angular momentum beam excitation using all-fiber weakly-fused mode selective coupler

S. PIDISHETY[1,2,*], S. PACHAVA[1,2], P. GREGG[3], S. RAMACHANDRAN[3], G. BRAMBILLA[2] AND B. SRINIVASAN[1]

1. Department of Electrical Engineering, Indian Institute of Technology Madras, Chennai 600036, India
2. Optoelectronics Research Centre, University of Southampton, Southampton, SO171BJ, United Kingdom
3. Electrical and Computer Engineering Department, Boston University, 8 St Mary's St, Boston, MA, USA

*Corresponding author: pd.shankara@gmail.com

OAM beam excitation through direct phase-matched coupling is experimentally demonstrated using an all-fiber weakly-fused mode selective coupler consisting of a single mode fiber and a ring-core fiber. Experimental results showing the excited OAM mode purity of up to 75% measured through the standard ring technique not only demonstrates the proof of concept, but also provides a baseline for further improvement.

© 2017 Optical Society of America

OCIS codes:(060.2310) Fiber optics; (230.1150) Optical devices; (050.4865) Optical vortices.

http://dx.doi.org/...

Optical beams with electric fields characterized by $\exp(il\phi)$, where ϕ is the azimuthal angle around the optical axis, and l is the topological charge, carry a well-defined orbital angular momentum (OAM) [1]. Due to their unique characteristics, such beams have been a subject of much interest for a variety of fundamental research studies and modern applications including optical manipulation [2,3], high resolution microscopy [4], surface-plasmon excitation [5] and next-generation optical communications networks [6,7]. Driven by such applications, the generation of OAM beams has been widely studied through free space techniques such as spiral phase plates [8], spatial light modulators (SLMs) [9], computer-generated holograms [10], cylindrical lens pairs [11], q-plates [12] and to a limited extent, optical fibers [13–17]. However, since all these techniques rely on free space optical beams and high-precision fiber coupling they require high tolerance fabrication and implementation. Hence, it is highly desirable to identify alternative all-fiber based techniques, potentially requiring no alignment sensitive components that enable direct excitation of desired OAM modes from a traditional Gaussian mode and are mode-scalable. Recently, preliminary demonstration of an approach to realize an all-fiber OAM mode excitation has been reported [15].

In this paper, we experimentally demonstrate an alternative all-fiber technique for the excitation of an OAM mode using a fused fiber coupler. Our approach is based on mode-selective coupling between different modes in two dissimilar fibers. Previously, such a technique has been used to achieve coupling between the fundamental HE_{11} mode in a single mode fiber (SMF) and a selected higher order LP-mode (HOM) group in a few mode fiber (FMF) [18,19]. However, the selective excitation of vector or OAM modes within a mode group in typical step-index FMFs cannot be achieved using such couplers, as the targeted modes in the FMF are nearly-degenerate with other OAM modes of the same $|l|$ (l>1) consisting of even/odd HE or EH eigenmodes, or, in the case of $l=1$, with the TE_{01}/TM_{01} modes. Since breaking such degeneracy in FMFs is essential for the excitation as well as stable propagation of the OAM modes [13], we chose a ring core fiber in our work. The ring core fiber breaks the degeneracy between the desired HE_{21} modes and neighboring TE_{01} or TM_{01} modes, thereby allowing the preservation of the excited OAM mode without significant intermodal coupling [13]. Phase matching between HE_{11} mode in the SMF and the desired mode in the ring core fiber can be achieved by pre-tapering the SMF and then fusing both fibers [17,18,20]. As such, it provides the promising alternative pathway to directly couple the traditional Gaussian beam to the desired OAM beams with high purity and good stability in an entirely integrated scheme. In addition, this all-fiber device could potentially generate OAM modes with higher charge as the above phase-matching technique could be extended to other OAM modes supported by the ring core fiber [21].

The index profile of the ring-core fiber used in our work is shown in Fig. 1. (a). The high index contrast and the annular ring guiding structure enable the stable propagation of neighboring vector modes that are usually nearly-degenerate in weakly guiding fibers, by achieving high effective index separation on the order of ($\Delta n_{eff} \sim 10^{-4}$) at $\lambda=1550$nm as shown in Fig. 1. (b). When the near-degeneracy between the different vector modes is removed, such modes have been shown to propagate $\sim$km lengths with low crosstalk [7].

As index profiles of selected fibers for coupler design are dissimilar, the effective index (n_{eff}) of the HE_{11} in the SMF is different from that of the target OAM ($HE_{21}^{e/o}$) mode in the ring-core fiber. Efficient coupling between the HE_{11} in the SMF and the target OAM mode ($HE_{21}^{e/o}$) in the ring-core fiber requires that modes have the same n_{eff}, i.e. they are phase matched [17].
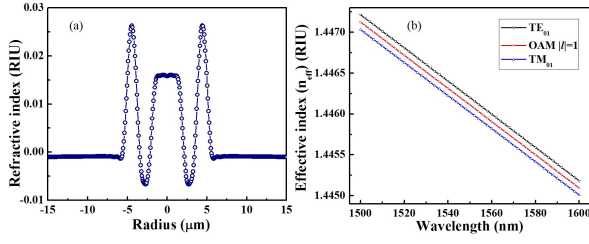
Fig. 1. (a): Experimentally measured refractive index profile of ring-core fiber at the wavelength λ=1550nm. The refractive index of silica is used as reference. (b): Effective index (n_{eff}) verses wavelength (simulations).

The phase matching condition was studied using the COMSOL Multiphysics® eigenmode solver to estimate the required ratio between the cladding diameter of the SMF and that of the ring-core fiber. A multi-layer configuration consisting of the two fiber cores, claddings and air region was adopted in the simulations. It is important that the air region is included in the simulations, as the evanescent field extends beyond the fiber cladding for small taper diameters. Fig. 2 shows n_{eff} for the HE_{11} mode in the SMF and for the OAM $|l|=1$ mode in the ring-core fiber, mapped as a function of fiber cladding diameter (d). The n_{eff} of neighboring modes i.e. TE_{01} and TM_{01} are also shown, and these results indicate that they remain sufficiently separated from the n_{eff} of the desired modes so as to enable preferential coupling to only the desired mode. Although a local electrical field superposition of TE and TM can be an OAM state, it is never a propagating fiber mode since TE and TM are not degenerate. Thus, these modes are considered parasitic for our devices. Since each circular polarization of the input HE_{11} mode couples preferentially to one of the two degenerate HE_{21} modes of the ring-core fiber, controlling the input polarization state using the PC enables exciting the desired OAM state via:

$$OAM^{\pm}_{11} = HE_{21}^{even} \pm iHE_{21}^{odd} = E(r)\{\sigma^{\pm} \exp(\pm il\phi)\} \qquad (1)$$

where σ is circular polarization with +/- corresponding to left and right circular polarization respectively, $E(r)$ is the electric field and l is charge of the OAM mode. As indicated with red-dashed lines in Fig. 2, the HE_{11} in the SMF has n_{eff} = 1.36 at a tapered cladding diameter of d_{SMF}~2.25 μm, while the OAM mode in the ring-core fiber shows the same n_{eff} at the tapered cladding diameter $d_{ring-core}$ ~ 3.58 μm. Therefore, the target diameter ratio ($\rho = d_{SMF}/d_{ring-core}$) should be ~ 0.63, implying that the SMF should be pre-tapered with respect to the ring-core fiber diameter before fusing. The required pre-tapered diameter for the SMF was calculated to be d_{SMF} = 56.5 μm, considering the ring-core fiber cladding diameter of $d_{ring-core}$ = 90 μm.
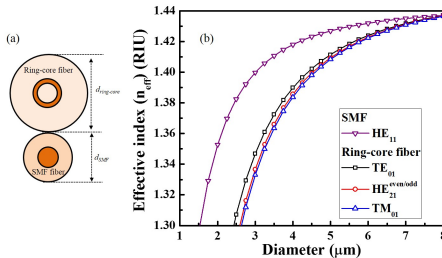

Fig. 2. (a) Approximate cross-section of the coupler showing tapered cladding diameter of SMF d_{SMF}~2.25 μm and of the ring-core fiber d_{ring-}

$_{core}$ ~ 3.58 μm. (b): Effective index (n_{eff}) of HE_{11} mode in the SMF and different modes (TE_{01}, OAM $|l|=1$ and TM_{01}) in the ring-core fiber mapped as function of the fiber cladding diameter.

Based on the above analysis and the simulations shown in Fig. 2, a conventional telecom-grade SMF (Elliot Scientific, SMF-1300/1500 core/cladding diameter = 8.2/125 μm, NA = 0.14) was adiabatically pre-tapered at ~1400 °C to the calculated diameter of d_{SMF} ~ 56.5±0.1 μm. The pre-tapering was performed using a custom-built fiber tapering rig consisting of a ceramic micro heater (NTT-AT, Japan) and high resolution translation stages [22]. The insertion loss of the pre-tapered fiber was measured to be less than ~0.1 dB.

The pre-tapered SMF was adjacently aligned with the un-tapered, straight ring-core fiber carefully without any twists and fixed together using UV-curable glue. The coupler was fabricated using the modified flame brushing technique [17,20,22] by using the same tapering rig. During pulling, the fibers weakly fuse, resulting in power transfer from the SMF into the ring-core fiber. The power from the output of both fibers was monitored and, the tapering and fusing procedure was stopped when the ratio of the power measured out of the ring-core fiber to that from the SMF reaches a peak value before starting to trail off. To identify this transition point, we repeated the fabrication process several times while observing the above power values. The resultant coupling length of the device was measured to be 14±0.2 mm. The fabricated coupler was handled using a stable supporting base plate and packaged in a plastic tube to ensure the excitation conditions to be unchanged and minimize the influence of environmental perturbations. Subsequently, the output beam from the ring-core fiber was analyzed using the characterization setup described below.
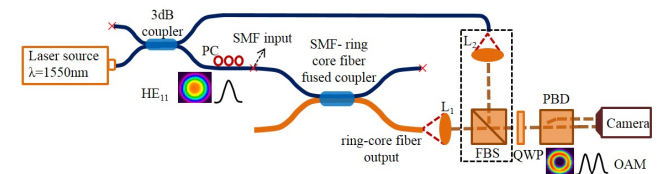

Fig. 3. Experimental setup for characterizing the generated OAM beam: solid lines are propagation path of light through the fiber; dashed lines are that of light through free space. PC-polarization controller, L_1 and L_2-collimating lens, FBS-free space beam splitter, QWP-quarter wave plate and PBD-polarization beam displacer.

The schematic diagram of the experimental setup used for characterization of the fabricated fused coupler is shown in Fig. 3. Light from a 1550-nm laser source (spectral width ~0.08 nm) was split into two arms using a commercial 3 dB coupler. Light in the other arm of the 3 dB coupler was used as a reference for the interference setup to analyze the OAM beam at the output of the fused coupler. The collimated (with f = 6 mm lens) output beam from the ring-core fiber was imaged using a CCD camera (MicronViewer-7290A). The output beam from the reference SMF and ring-core fiber (cleaved at ~40 cm beyond the interaction region of coupler) were combined using a free space beam splitter to form the interference pattern. The interference setup (shown in dotted line box) was used to determine the charge ±l number of

the generated OAM mode by observing its characteristic fork and spiral patterns as shown in Fig. 4 (b and c).

A clear doughnut pattern out of the ring-core fiber, shown in Fig. 4, is achieved by fine tuning the input polarization, when the reference arm (Gaussian) is blocked and without the polarization displacer on the beam path. The absence of a Gaussian intensity pattern, and a relatively uniform azimuthal intensity distribution qualitatively suggests that phase matched coupling to one of the vector HOMs (OAM, TE_{01} and TM_{01}) modes was achieved without substantial coupling to the neighboring vector modes, or to HE_{11}.
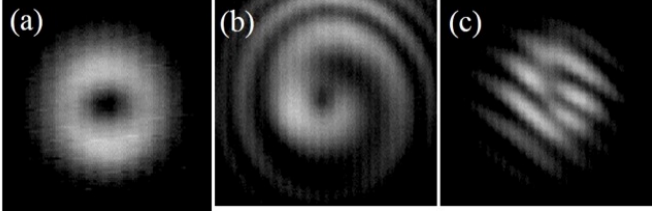

Fig. 4. (a): Far field image of the generated OAM beam. (b) & (c): characteristic spiral and fork interference patterns of OAM beam and Gaussian reference, respectively.

At fixed input polarization conditions, a polarization measurement performed using a polarizer and quarter wave plate combination [5,17,23] revealed that the output beam was uniformly circularly polarized (~86%), further suggesting that the generated output beam was predominantly an OAM mode. With the beam from the reference arm incident on the camera co-aligned with that from the ring-core fiber, we observe the characteristic spiral interference pattern between an OAM and an expanded Gaussian beam as shown in Fig. 4 (b). Further, with the reference arm incident on the camera at a slight angle with respect to the beam from the ring-core fiber, we observe the characteristic fork interference pattern between the OAM and the unexpanded Gaussian beam as shown in Fig. 4 (c), indicating that the charge of generated OAM beam is $l = \pm 1$.

The above spiral and fork patterns are characteristic of a OAM mode, but are not sufficient to prove that the output beam corresponds to an OAM mode since both TE and TM can yield spiral interferograms under certain conditions [24]. To confirm the OAM mode excitation as well as to estimate the purity of the mode, the output beam was analyzed further by the Ring technique [14] as discussed below.

The 1550 nm laser source was replaced with a narrow-bandwidth wavelength tunable external cavity laser (ECL), while the fiber output was imaged through a circular polarization beam splitter. The input polarization was chosen such that the output beam resembles a donut pattern, and images were taken as a function of wavelength (λ). For each image, the intensity pattern was deconstructed into an azimuthal Fourier series, from which relative modal weights could be determined [14] as shown in Fig. 5. Note that the power measured in the HE_{11} mode is limited by the noise floor in our measurement, corresponding to ~1%. Based on this analysis, we estimate a maximum modal purity of ~75% and an average purity of ~72% over 1 nm. As seen in Fig. 5, the purity of OAM mode is affected by the spurious light coupling into unwanted neighboring modes (TE_{01} and TM_{01}). This may be

attributed to a possible deviation in target diameters of the two fibers, which are difficult to track in a fused coupler.
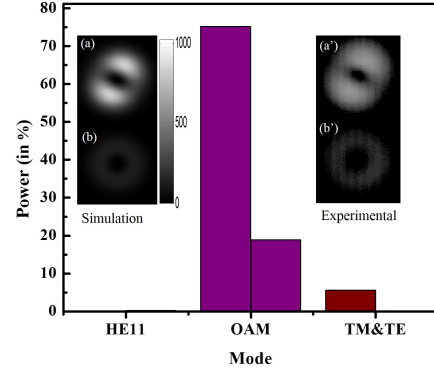

Fig. 5. Purity measurement of the OAM beam: modal content (HE_{11}, OAM $|l|$=1 and TE_{01}, TM_{01}) of ring-core fiber output. Inset: Simulation and experimental images of RCP and LCP projection of OAM mode.

Furthermore, the spectral dependence of the OAM mode purity was investigated over a ~2 nm as shown in Fig. 6. Although the coupler output exhibits noticeable performance variation as a function of wavelength, the achieved OAM purity of 72% over a ~1 nm window is reasonably stable.

The strong spectral dependence mentioned above is not expected from a perfectly fused coupler even if its target diameters are incorrect. If, on the other hand, the degree of fusion between the two fibers is not uniform [25], one could obtain a multi-cascaded coupler that could potentially be wavelength sensitive. Since it is not straightforward to independently measure the uniformity of the coupler, we simulate the above spectral dependence using the transfer matrix method. Such simulations are carried out by modeling the device as two cascaded couplers with an arbitrary phase delay (θ) corresponding to a length difference between the two arms as a free parameter. In this relatively simple scalar model, we consider power coupling from the HE_{11} [e/o] mode in the tapered SMF to HE_{21} [e/o] mode in the tapered ring-core fiber and estimated the coupling co-efficient (κ) as [26].

$$\kappa = \frac{\omega^2}{2\beta_2 c^2} \frac{\iint E_1(x,y)_{\delta n^2(x,y)} E_2^*(x,y) dx dy}{\iint |E_2(x,y)|^2 dx dy} \quad (2)$$

where ω is the optical angular frequency, E_1, E_2 are electric fields corresponding to the HE_{21} [e/o] modes in tapered ring-core fiber and the HE_{11} [e/o] modes in the tapered SMF respectively and β_2 is propagation constant of HE_{11} [e/o] mode in SMF, δn is the index perturbation due to the presence of the ring-core fiber and c is the speed of light. The transfer matrix for the cascaded fused coupler describing the interaction of the HE_{21} [e/o] modes in tapered ring-core fiber and the HE_{11} [e/o] modes in the tapered SMF is given by [26]

$$\begin{bmatrix} cos(\kappa L) & -isin(\kappa L) \\ -isin(\kappa L) & cos(\kappa L) \end{bmatrix} \begin{bmatrix} 1 & 0 \\ 0 & e^{i\theta} \end{bmatrix} \begin{bmatrix} \cos(\kappa L) & -isin(\kappa L) \\ -i\sin(\kappa L) & \cos(\kappa L) \end{bmatrix} \quad (3)$$

where L is the individual coupler length. By varying the parameters κ, L, θ for the two cascaded couplers, the experimental spectrum was fitted with simulations. The best possible fit was obtained for the parameters $\kappa = 745.38 – 746.06/cm$, $L = 9.7\ mm$ for both the couplers with a delay of $\theta = \pi/3$ radians between them. Such a phase delay corresponds to a length difference of ~0.16 μm, which could arise due to non-optimal fusing of the coupler.
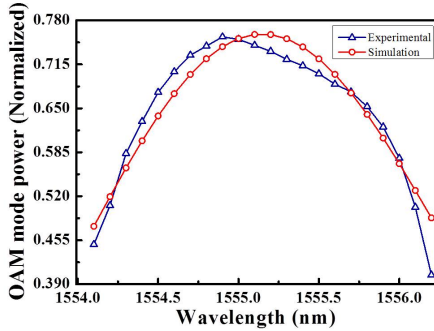

Fig. 6. The power of coupled OAM mode as a function wavelength: experimental and simulations fit.

As shown in Fig. 6, the experimental results which have an error bar of roughly 5% are quite consistent with simulations indicating that the spectral dependence of the coupler performance was probably due to the non-uniform degree of fusion. Since spectral and polarization dependence arise from similar coupling and detuning variations in fused couplers [25], the non-uniform degree of fusion discussed above could also explain the noticeable polarization dependence observed for our device. The measured coupling efficiency of ~75% could be improved further by optimizing the coupler degree of fusion and associated coupler length. Only a very small (~3%) variation of the spatial intensity distribution of the generated modes is measured after more than 45 minutes, indicating good stability of the device.

In summary, we experimentally demonstrated for the first time to the best of our knowledge, an all-fiber fused coupler for the selective excitation of an OAM mode ($l = 1$) in a ring-core fiber. In the weakly-fused coupler, a precisely pre-tapered standard SMF and a ring-core fiber were fused together to achieve the required phase matching. Detailed measurements and analysis of the excited mode show that an average modal purity of ~72% is achieved over a spectral range of 1 nm with less than 6 dB insertion loss. Our device is a proof of demonstration of a compact, viable, all-fiber means of generating OAM modes. While the purity and loss values for our device would require further optimization, simulations on our device suggest that the primary path for improvement lies in the better control of our coupler fusion process. Since this fabrication technique is a well-established industry standard for realizing fused fiber couplers, we expect significant improvement in the loss and purity. Crucially, this device provides a pathway towards achieving excitation of OAM modes with higher charges.

References
1. A. M. Yao and M. J. Padgett, Adv. Opt. Photonics **3**, 161 (2011).
2. J. E. Curtis and D. G. Grier, Phys. Rev. Lett. **90**, 133901 (2003).
3. J. W. R. Tabosa and D. V. Petrov, Phys. Rev. Lett. **83**, 4967 (1999).
4. L. Yan, P. Gregg, E. Karimi, A. Rubano, L. Marrucci, R. Boyd, and S. Ramachandran, Optica **2**, 900 (2015).
5. S. Pidishety, V. Kumar, and N. K. Viswanathan, Opt. Lett. **37**, 4233 (2012).
6. J. Wang, J.-Y. Yang, I. M. Fazal, N. Ahmed, Y. Yan, H. Huang, Y. Ren, Y. Yue, S. Dolinar, M. Tur, and A. E. Willner, Nat. Photonics **6**, 488 (2012).
7. N. Bozinovic, Y. Yue, Y. Ren, M. Tur, P. Kristensen, H. Huang, A. E. Willner, and S. Ramachandran, Science **340**, 1545 (2013).
8. M. W. Beijersbergen, R. P. C. Coerwinkel, M. Kristensen, and J. P. Woerdman, Opt. Commun. **112**, 321 (1994).
9. A. Cofré, P. García-Martínez, A. Vargas, and I. Moreno, Eur. J. Phys. **38**, 14005 (2017).
10. N. R. Heckenberg, R. McDuff, C. P. Smith, and A. G. White, Opt. Lett. **17**, 221 (1992).
11. M. W. Beijersbergen, L. Allen, H. E. L. O. van der Veen, and J. P. Woerdman, Opt. Commun. **96**, 123 (1993).
12. L. Marrucci, C. Manzo, and D. Paparo, Phys. Rev. Lett. **96**, 163905 (2006).
13. S. Ramachandran, P. Kristensen, and M. F. Yan, Opt. Lett. **34**, 2525 (2009).
14. N. Bozinovic, S. Golowich, P. Kristensen, and S. Ramachandran, Opt. Lett. **37**, 2451 (2012).
15. Z. S. Eznaveh, J. C. A. Zacarias, J. Antonio-Lopez, Y. Jung, K. Shi, B. C. Thomsen, D. Richardson, S. G. Leon-Saval, and R. A. Correa, in *Opt. Fiber Commun. Conf. 2017 Pap. Tu3J3* (Optical Society of America, 2017), p. Tu3J.3.
16. V. V. G. Krishna Inavalli and N. K. Viswanathan, Opt. Commun. **283**, 861 (2010).
17. S. Pidishety, B. Srinivasan, and G. Brambilla, IEEE Photonics Technol. Lett. **29**, 31 (2017).
18. R. Ismaeel, T. Lee, B. Oduro, Y. Jung, and G. Brambilla, Opt. Express **22**, 11610 (2014).
19. K. J. Park, K. Y. Song, Y. K. Kim, J. H. Lee, and B. Y. Kim, Opt. Express **24**, 3543 (2016).
20. S. Pidishety, M. I. Abdul Khudus, P. Gregg, S. Ramachandran, B. Srinivasan, and G. Brambilla, in (OSA, 2016), p. STu1F.2.
21. S. Pidishety, S. Pachava, P. Gregg, A. McGuffin, S. Ramachandran, G. Brambilla, and B. Srinivasan, in *13th Int. Conf. Fiber Opt. Photonics 2016 Pap. W2G4* (Optical Society of America, 2016), p. W2G.4.
22. G. Brambilla, J. Opt. **12**, 43001 (2010).
23. S. Pidishety and N. K. Viswanathan, JOSA B **30**, 806 (2013).
24. P. Gregg, M. Mirhosseini, A. Rubano, L. Marrucci, E. Karimi, R. W. Boyd, and S. Ramachandran, Opt. Lett. **40**, 1729 (2015).
25. K. Morishita and K. Yamazaki, J. Light. Technol. **29**, 330 (2011).
26. Amnon Yariv, Photonics - Hardcover Oxford University Press.

References (in full)

1. A. M. Yao and M. J. Padgett, "Orbital angular momentum: origins, behavior and applications," Adv. Opt. Photonics **3**, 161 (2011).

2. J. E. Curtis and D. G. Grier, "Structure of optical vortices," Phys. Rev. Lett. **90**, 133901 (2003).

3. J. W. R. Tabosa and D. V. Petrov, "Optical Pumping of Orbital Angular Momentum of Light in Cold Cesium Atoms," Phys. Rev. Lett. **83**, 4967–4970 (1999).

4. L. Yan, P. Gregg, E. Karimi, A. Rubano, L. Marrucci, R. Boyd, and S. Ramachandran, "Q-plate enabled spectrally diverse orbital-angular-momentum conversion for stimulated emission depletion microscopy," Optica **2**, 900–903 (2015).

5. S. Pidishety, V. Kumar, and N. K. Viswanathan, "Plasmon-mediated vectorial topological dipole: formation and annihilation," Opt. Lett. **37**, 4233–4235 (2012).

6. J. Wang, J.-Y. Yang, I. M. Fazal, N. Ahmed, Y. Yan, H. Huang, Y. Ren, Y. Yue, S. Dolinar, M. Tur, and A. E. Willner, "Terabit free-space data transmission employing orbital angular momentum multiplexing," Nat. Photonics **6**, 488–496 (2012).

7. N. Bozinovic, Y. Yue, Y. Ren, M. Tur, P. Kristensen, H. Huang, A. E. Willner, and S. Ramachandran, "Terabit-Scale Orbital Angular Momentum Mode Division Multiplexing in Fibers," Science **340**, 1545–1548 (2013).

8. M. W. Beijersbergen, R. P. C. Coerwinkel, M. Kristensen, and J. P. Woerdman, "Helical-wavefront laser beams produced with a spiral phaseplate," Opt. Commun. **112**, 321–327 (1994).

9. A. Cofré, P. García-Martínez, A. Vargas, and I. Moreno, "Vortex beam generation and other advanced optics experiments reproduced with a twisted-nematic liquid-crystal display with limited phase modulation," Eur. J. Phys. **38**, 14005 (2017).

10. N. R. Heckenberg, R. McDuff, C. P. Smith, and A. G. White, "Generation of optical phase singularities by computer-generated holograms," Opt. Lett. **17**, 221–223 (1992).

11. M. W. Beijersbergen, L. Allen, H. E. L. O. van der Veen, and J. P. Woerdman, "Astigmatic laser mode converters and transfer of orbital angular momentum," Opt. Commun. **96**, 123–132 (1993).

12. L. Marrucci, C. Manzo, and D. Paparo, "Optical Spin-to-Orbital Angular Momentum Conversion in Inhomogeneous Anisotropic Media," Phys. Rev. Lett. **96**, 163905 (2006).

13. S. Ramachandran, P. Kristensen, and M. F. Yan, "Generation and propagation of radially polarized beams in optical fibers," Opt. Lett. **34**, 2525 (2009).

14. N. Bozinovic, S. Golowich, P. Kristensen, and S. Ramachandran, "Control of orbital angular momentum of light with optical fibers," Opt. Lett. **37**, 2451 (2012).

15. Z. S. Eznaveh, J. C. A. Zacarias, J. Antonio-Lopez, Y. Jung, K. Shi, B. C. Thomsen, D. Richardson, S. G. Leon-Saval, and R. A. Correa, "Annular Core Photonic Lantern Spatial Mode Multiplexer," in *Optical Fiber Communication Conference (2017), Paper Tu3J.3* (Optical Society of America, 2017), p. Tu3J.3.

16. V. V. G. Krishna Inavalli and N. K. Viswanathan, "Switchable vector vortex beam generation using an optical fiber," Opt. Commun. **283**, 861–864 (2010).

17. S. Pidishety, B. Srinivasan, and G. Brambilla, "All-Fiber Fused Coupler for Stable Generation of Radially and Azimuthally Polarized Beams," IEEE Photonics Technol. Lett. **29**, 31–34 (2017).

18. R. Ismaeel, T. Lee, B. Oduro, Y. Jung, and G. Brambilla, "All-fiber fused directional coupler for highly efficient spatial mode conversion," Opt. Express **22**, 11610 (2014).

19. K. J. Park, K. Y. Song, Y. K. Kim, J. H. Lee, and B. Y. Kim, "Broadband mode division multiplexer using all-fiber mode selective couplers," Opt. Express **24**, 3543 (2016).

20. S. Pidishety, M. I. Abdul Khudus, P. Gregg, S. Ramachandran, B. Srinivasan, and G. Brambilla, "OAM Beam Generation using All-fiber Fused Couplers," in (OSA, 2016), p. STu1F.2.

21. S. Pidishety, S. Pachava, P. Gregg, A. McGuffin, S. Ramachandran, G. Brambilla, and B. Srinivasan, "Investigation of scalability of all-fiber fused mode selective coupler for generating multiple OAM states," in *13th International Conference on Fiber Optics and Photonics (2016), Paper W2G.4* (Optical Society of America, 2016), p. W2G.4.

22. G. Brambilla, "Optical fibre nanowires and microwires: a review," J. Opt. **12**, 43001 (2010).

23. S. Pidishety and N. K. Viswanathan, "Polarimetric measurement of optically perturbed surface plasmonic field," JOSA B **30**, 806–811 (2013).

24. P. Gregg, M. Mirhosseini, A. Rubano, L. Marrucci, E. Karimi, R. W. Boyd, and S. Ramachandran, "Q-plates as higher order polarization controllers for orbital angular momentum modes of fiber," Opt. Lett. **40**, 1729–1732 (2015).

25. K. Morishita and K. Yamazaki, "Wavelength and Polarization Dependences of Fused Fiber Couplers," J. Light. Technol. **29**, 330–334 (2011).

26. Photonics - Amnon Yariv; Pochi Yeh - Oxford University Press.